LA-UR-23-20486

Approved for public release; distribution is unlimited.

Title:	Role of heating and turbulent heat transfer in HE burning and detonation
Author(s):	Chang, Chong Scannapieco, Anthony J.
Intended for:	Report
Issued:	2023-01-18

January 5, 2023

Role of heating and turbulent heat transfer in HE burning and detonation

C. H. Chang and A. J. Scannapieco

Los Alamos National Laboratory

Enhanced heat transfer model has been developed due to the turbulence in the cracks and pores in the burning fractured HE. This turbulence then serves in the initialization of the turbulence in the product gas. Enhanced heat transfer is also modeled in the turbulent product gas. Numerical simulations of the onset of HE burning and transition to detonation have been performed with and without the turbulent heat transfer model. Computational results indicate that onset of chemical reactions and transition to detonation is induced by the shockwave formed by the pressure rise caused by the heating. In other words, processes similar to shock-to-detonation transition (SDT) could become the driving mechanism for HE explosion and detonation in the case of heating rather than the temperature alone.

I. INTRODUCTION

High explosive burning and detonation can be caused by applying a pressure force and/or heating. Applying pressure forces have been commonly used in HE applications. For example, hitting by a firing pin is a common method of igniting bullet propellant. Of course, heating or temperature rise has also been used in HE applications. Gun powder is commonly ignited by fire.

Numerical simulation of flame acceleration (FA) and transition to detonation has recently been presented [1]. Included in the model are a chemical reaction chain proposed by Henson and Smilowitz [2], equation-of-state (EOS) of all species involved in the reaction chain [3], visco-plastic statistical crack mechanics (VPSCRAM model [4]), and a multiphase hotspot model [5]. These models are integrated in the reacting flow code BABBO capable of handling an arbitrary number of species and reactions with consistent multi-species EOS. Note that the cause of HE explosion discussed in Ref. [1] is the hitting or application of the pressure force.

The case of heating is more complicated than the case of hitting, since temperature rise is almost always accompanied by the pressure rise which could affect the ignition of HE and transition to detonation. That is, hitting and heating simultaneously act on the HE explosion, making it difficult to analyze heating effects without involving hitting.

Fortunately, isolation of heating from hitting appears to be possible to some degree due to the disparity in time scales. When a portion of HE is uniformly heated, HE is expected to expand, causing a pressure rise in that portion. This pressure rise will then propagate into the rest of the HE at the speed of sound. Since the heated portion of HE continues expanding, acting like the accelerating piston in a shock tube, a pressure wave front will accumulate, eventually forming a shockwave. Due to the required accumulation, the shockwave formation is expected from a distance away from the heated region. Since

heat transfer is a much slower process than sound propagation, the heating originated from the heated region is expected to be absent at the the location of the shockwave formation.

Heating effects can be observed in the region next to the heated region, where the temperature will rise due to the heat transfer from the heated portion, initiating the HE burning. The pressure rise in this region is somewhat slow and uniform, since the pressure wave has passed through before any substantial heating occurs. Therefore, contributions due to the pressure force (gradient) can be neglected for the present purpose. In summary, effects of the hitting and heating are expected to manifest at different locations, making it possible to make separate observations.

HE burning spreads into the unburned HE. When burning flame accelerates, HE burning is expected to make the transition to detonation [1]. One of our objectives is to computationally analyze and compare contributions of heating and hitting to the onset of HE burning, FA, and transition to detonation. It is then necessary to include a heat transfer model that accounts for the turbulence.

The rate of heating is determined by the heat transfer from the heated portion. Needless to say, heat transfer is controlled by the HE morphology. HE initially is a solid material containing pores and cracks, and heat is transferred by conduction. As HE temperature increases, vaporization and decomposition of the solid HE would occur at the surface of pores and cracks, filling the void. At this stage, little burning reaction is expected. The gas is expected to flow through the pores and cracks due to the pressure force created by the evaporated HE, and HE burning reactions commence. At this stage, the dominating heat transfer mechanism is convection created by the motion of the gas in pores, even at a small porosity. That is, HE already is in the "convective burn" regime. Release of the chemical energy becomes a major source of the temperature rise at this point. As the porosity increases, flow in the pore would become turbulent, further enhancing the heat transfer. This turbulence will continue when HE is completely vaporized and chemical reactions are complete.

The anticipated sequence of events is summarized as follows:

1. A portion of HE is heated.

2. Temperature and pressure rise in that portion.

3. Both temperature and pressure rise start propagating into the unheated region. But the pressure wave outruns the temperature rise.

4. Pressure wave accumulates, and a shockwave forms at some distance away from the heated region.

5. Shockwave ignites HE. This process is similar to the initial stage of SDT. In the mean time, HE next to the heated region may also be ignited by the temperature rise.

6. Initially heat conduction plays a role, but convective heat transfer dominates heat conduction as soon as HE evaporation starts. This usually occurs very fast due to the hotspot formation.

7. Pores and cracks grow and turbulence develops, further enhancing heat transfer. Turbulent combustion takes place in pores and cracks.

8. When HE is completely evaporated, large-scale turbulence develops.

9. Assisted by heat transfer from the burning region, a flame may develop and accelerate, making the transition to detonation [1]. When FA occurs in the region where HE burning has been started by the shockwave, this transition process essentially is SDT.

Our objective is to computationally study this sequence and extend the previous heat transfer model [1] for the turbulence modeling involving transport and dissipation of the turbulent kinetic energy. In this report, we first introduce our extension to the heat transfer model for HE product gas and heat convection in pores and cracks of fractured HE. In the previous model, the heat transfer in the product gas was modeled by the Smargorinsky eddy viscosity model, which ignores the transport (advection) of turbulence from the upstream. Therefore, any source of turbulence in the fractured HE was ignored in the HE product gas. However, the strength of turbulence in the flow in the cracks can become non-negligible, as the porosity increases. (As HE burns, porosity increases rapidly.) In the present approach, the turbulence in the fractured HE serves as the initial turbulence of the product gas. To include this feature, the turbulence model needs to have the feature of transport and dissipation of turbulent kinetic energy. This feature is available in popular turbulence models such as the k-ϵ models [6–8]. In BABBO, the K-L model [9] is available, and thus the present formulation has been applied to the K-L model. A K-L model is used because it is often natural to define an initial scale length of the turbulence which is equaled to initial structure in the material. This is an advantage of the K-L model over k-ϵ models in situations where an initial value of ϵ is not easily defined. The present approach can of course be applied to other turbulence models of this type. We then apply the new heat transfer model to a case in which a portion of the HE is heated, and study the sequence above, followed by concluding remarks.

HE usually contains voids, pores, and cracks, and hotspots are expected to form when a pressure force causes pore collapse and/or friction in cracks. But our hotspot model [5] is in its infancy, and thus hotspot effects could be inadequately accounted for. Nonetheless, VPSCRAM model [4] and our current hotspot model [5] have been used to represent crack growth required for modeling of turbulence in cracks. Further study of hotspot effects will be carried out in due course, when an improved hotspot model becomes available.

II. TURBULENT HEAT TRANSFER IN FRACTURED HE

Turbulence can be developed as the size of the cracks and pores increase in fractured HE. This situation is always encountered in HE, since the volume fraction or porosity increases as HE burns. Definitions of the pore Reynolds numbers in various turbulent flows in porous media can be found in Ref. [10]. Length scales used in those Reynolds numbers include the hydraulic diameter, particle size, pore size, and permeability. We thus need to select the appropriate length scale for our purpose. We select the crack size since it is a natural length scale used in our fracture model [4]. The Reynolds number is then given by

$$Re = \frac{\rho_g |\mathbf{u}_g| c_s}{\mu_g} \tag{1}$$

where ρ_g and μ_g are respectively the density and dynamic viscosity of the burning HE gas, c_s is the crack size, and $\mathbf{u}_g$ is the gas velocity in the pore. The viscosity can be obtained

from the reported HE properties [11]. The velocity $\mathbf{u}_g$ can be obtained by solving Darcy's law with the Forchheimer term as discussed in Ref. [1].

Flow in porous media evolves through various regimes including Darcy regime, inertial regime, transitional regime, turbulent regime, and asymptotic regime [10]. These flow regimes generally corresponds to the magnitude of the Reynolds number. We expect that the Reynolds number used in the present formulation would produce reasonable values compared to the Reynolds numbers in Ref. [10]. We thus assume that the flow would be in a turbulent regime when $Re > Re_c$, where Re_c is the critical Reynolds number defined by the user. Typical values of Re_c is suggested to be approximately 500.

Our objective is to calculate the turbulent heat transfer coefficient when $Re > Re_c$. Since we are not modeling the flow in the fractured HE, information necessary for the estimation of the heat transfer coefficient is often unavailable. We thus calculate the eddy viscosity in the pores using the Smargorinsky model where turbulent kinematic viscosity is given by [12]

$$\nu_t = C_S^2 \Delta^2 |\mathsf{S}| \tag{2}$$

where C_S is the model constant, Δ is the spatial resolution usually given as the computational mesh size, and $|\mathsf{S}|$ is the Galilean invariant estimation of velocity differences over Δ. Since the flow in the pore is subzonal in nature, we use $\Delta \approx c_s$ and $|\mathsf{S}| \approx |\mathbf{u}_g|/c_s$.

The turbulent thermal conductivity is then given by

$$\lambda_t = \rho_g C_{pg} \frac{\nu_t}{\mathrm{Pr}_t} \tag{3}$$

where Pr_t is the turbulent Prandtl number, whose typical value is between 0.7 and unity, and C_{pg} is the specific heat of the gas. The heat flux is then calculated using λ_t as discussed in Ref. [1].

Transport modeling of turbulence implies that turbulence is generated, advected, and dissipated. In a simple two-equation turbulence model, this is typically represented by evolutions of the turbulent kinetic energy and its dissipation or length scale. That is, the Smargorinsky model used in Ref. [1] is not adequate for this approach. Since a K-L model is available in BABBO, the present discussion is limited to the K-L model. Application of the present discussion to other models should nonetheless be straightforward.

When the present model is used in the context of the K-L model, the eddy viscosity is given by [9]

$$\nu_t = c_\mu L \left(2K\right)^{1/2} \tag{4}$$

where $c_\mu = 0.4$ is the model constant used in the K-L model, and K and L respectively are the turbulent kinetic energy and length scale calculated in the K-L model. Note that $c_\mu = 0.4$ is different from the values listed in Ref. [9], but appears to produce better results. Initially, K is set as a fraction of the flow kinetic energy, and L is set as the crack size.

In BABBO, the K-L model is applied only to the materials with turbulence. For example, it is not applied to the solid HE. Therefore, K and L at the boundary of the HE product gas need to be specified. At the material boundary facing other materials, e.g., metal surfaces, we specify K and L in the usual manner: $K = 0$ and $\partial L/\partial x = 0$, where x is the coordinate direction normal to the surface. Initial values of K and L are set as input values.

At the boundary facing burning solid HE, we set K and L as discussed above. It is necessary to determine the zones facing the HE product. (Complete consumption of

the solid HE may take a number of zones. Among them, the turbulence quantities of the zones facing zones with HE product gas only, i.e., without solid HE, are used as the boundary conditions.) The turbulence quantities specified as the boundary conditions are then transported into the gaseous region, and used in the K-L model.

III. COMPUTATIONAL RESULTS

Details of the employed model ingredients, including the chemical reaction chain, equation-of-state (EOS), hotspot modeling, and VPSCRAM model, have been presented in the previous reports [4, 5, 13], and only the essential information is discussed here. The Henson-Smilowitz (HS) multi-reaction chain [2, 13] and species EOS provided by the MAGPIE project at LANL [3] have been used in all calculations. The calculation domain is a cylindrical HMX rod 11.0 cm long with 200 μm radius, subdivided by 1100×2 zones ($\Delta r = \Delta z = 100\mu$m). One end of the rod, occupying one hundred zones (1.0 cm), receives uniform heating of 5×10^5 kJ/(cc-sec) for the duration of 4.0 μsec. The initial temperature is 300 K. The Neumann boundary conditions with zero fluxes are used at the axis, around the cylinder, and the heated end of the rod, while an open boundary is used for the non-heated end of the rod. (This implies that a one-dimensional problem has been solved in a two-dimensional domain in the present calculation. It is necessary to test the VPSCRAM model in a higher dimension than one. The turbulent heat transfer model should also be assessed in more than one dimension. A three-dimensional (3-D) domain would eventually be necessary. 3-D calculations will be carried out in the future, and those results will be reported in due course.)

We first carried out a simulation without turbulent heat transfer. Heat conduction was active. The thermal conductivity was obtained from Ref. [11] as discussed in Ref. [1]. Figure 1 shows temperature and pressure profiles during early stages of the HE burning. Temperature in the heated region has substantially increased. It also shows that expansion is taking place. Pressure rise initially propagates without formation of a shockwave as shown at 0.58 and 1.28 μsecs in Fig. 1. At a later time, pressure waves accumulate, forming a shockwave due to the continued expansion.

Temperature profiles shown in Fig. 1 suggest that there is little HE burning at the leading edges of the pressure pulses, which is confirmed by Fig. 2. Note that black lines represents the HMX mass fractions of cold and hot phases. When both phases exist simultaneously, two black lines are present. Figure 2 show that HE burning at 2.58 μsec is slow between the leading edge of the pressure pulse and the edge of the heated region, and that HE burning takes place in response to the temperature increase. Chemical reactions at this point do not appear to lead the temperature increase.

When rapid HE burning starts, both temperature and pressure show an increase as shown in Fig. 3. Note that two peaks in both temperature and pressure are shown in at 3.88 (green) and 4.18 (blue) μsec. The first (left) peak develops first as shown in profiles at 3.58 (black) and 3.78 (red), and it represents the combustion of evaporated HMX. Note that temperature rise here is not caused by the heating from the heated region, rather, it is caused by the compression associate with the pressure rise (pressure rise here is larger than the heated region as shown in Fig. 3). The second (right) peak is produced by the burning of HMX due to the rapid pressure rise (shock heating) and the associated temperature rise. The leading (right) side of the second peak represents the initial heating and burning due to

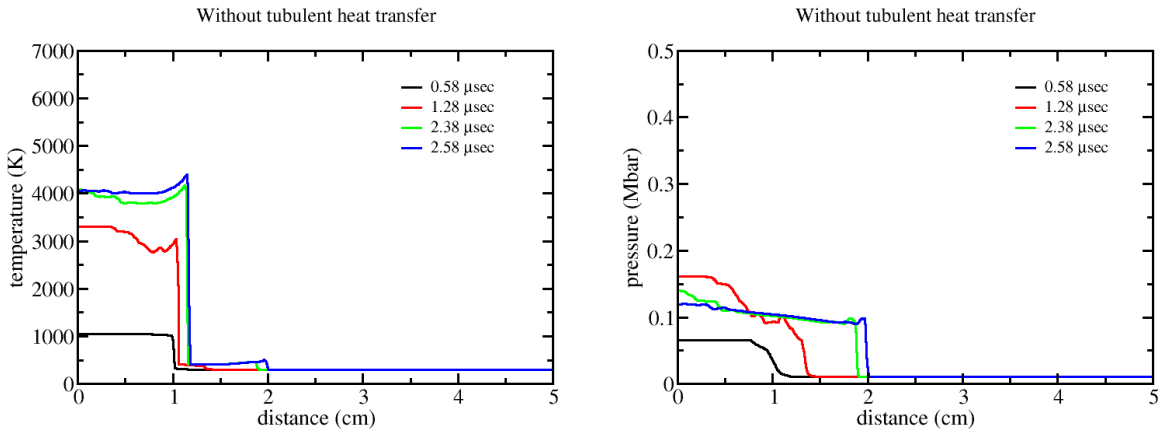

FIG. 1. Temperature and pressure profiles at 0.58, 1.28, 2.38, and 2.58 μsec with thermal conduction only.

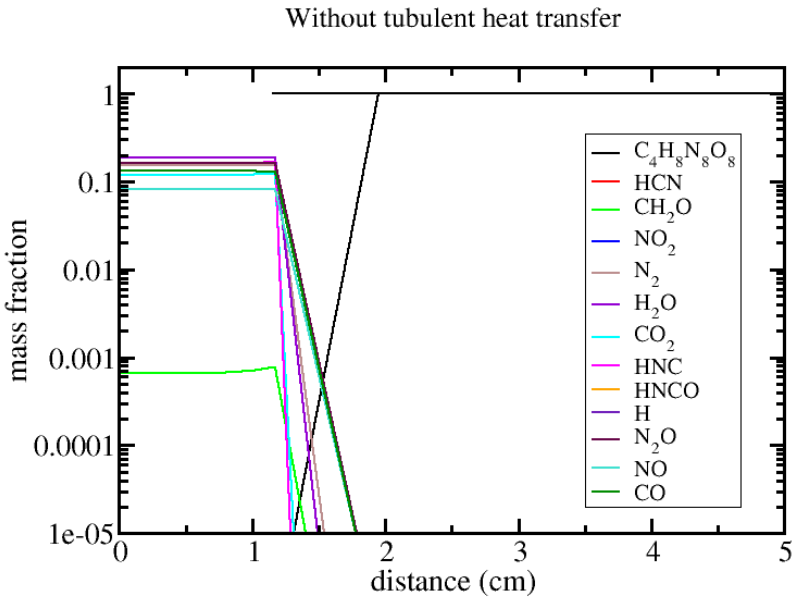

FIG. 2. Species mass fraction profiles at 2.58 μsec with thermal conduction only.

the first shockwave. This is immediately followed by a much stronger shockwave, referred to as the "flame shock" here, which actually represents detonation of the partially burned HE as shown by the profiles at 4.38 μsec (brown). The flame formation and acceleration behavior of the second peak show essentially identical behavior discussed in transition to detonation due to hitting discussed in Ref. [1]. Note that the first peak represents the burning in the downstream of the second peak. Since reactants are consumed by the second peak, the first peak becomes weaker. This shows that SDT occurs in the case of heating.

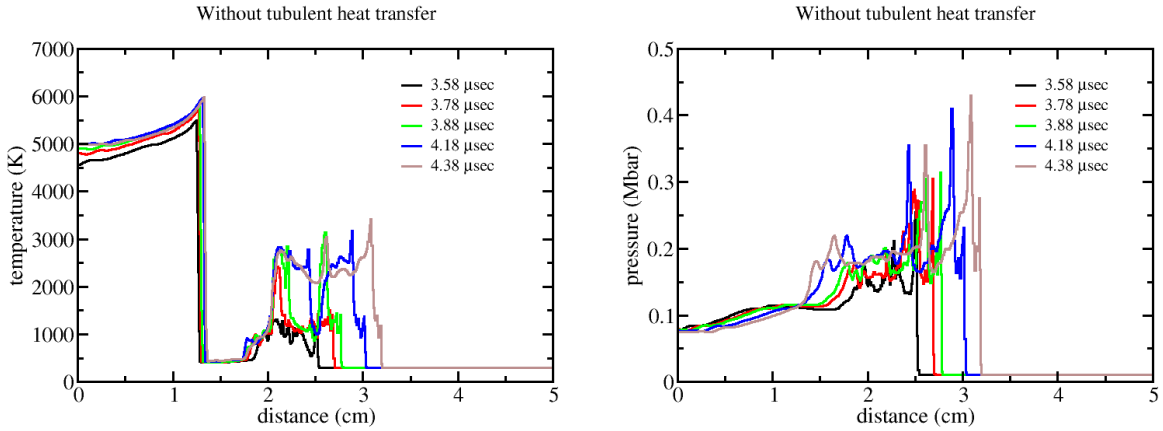

FIG. 3. Temperature and pressure profiles at 3.58, 3.78, 3.88, 4.18 and 4.38 μsec with thermal conduction only.

In order to reduce the shockwave effects, it is necessary to make the shockwave formation much slower. This may be accomplished by very slow heating. However, once chemical reactions start in the heated region, rapid temperature rise would occur, sending the pressure wave into the unburnt HE. This pressure wave would form a shockwave, driving the flame formation, FA, and transition to detonation. That is, SDT-like process would still be the driving mechanism.

Species mass fraction profiles at 3.88 μsec are shown in Fig. 4. They show the presence of two main reaction regions. For example, CO (dark green) and NO_2 (blue) profiles respectively show two valleys and peaks between 2.2 and 2.6 cm, consistent with the temperature profiles shown in Fig. 3.

Figure 5 shows a development of a detonation wave by merging the leading and flame shock as discussed above. Again, identical behavior is shown in the transition to detonation due to hitting (SDT) discussed in Ref. [1]. However, unlike the case of hitting, small high temperature pulses follow behind the detonation waves. They are the first temperature peak that is gradually weakening, due to the consumption of reactants by the leading flame shock.

Species mass fraction profiles at 6.08 μsec are shown in Fig. 6. Identifiable reaction regions are: (1) a detonation region at around 4.7 cm, (2) an unburned and slow-burning region between 1.5 and 2.0 cm, and (3) a heated region between 0.0 and 1.5 cm. Species mass fractions in region (3) are essentially identical to the ones shown in Fig. 2. The slopes shown at around 1.5 cm represent the slow HE burning as the heated region spreads. (Slopes at 4.7 cm show the fast detonation.) The slopes between 1.8 and 2.0 cm represent the consumption of the unburned region as the unburned region is following the flame region. Slopes of both sides show relatively slow progress of chemical reactions.

Figure 7 shows species mass fractions around the detonation wave (4.7 cm in Fig. 6) at 6.08 μsec. Species mass fractions of only the hotspot phase are shown in Fig. 6. Discontinuities at 4.74 cm are caused by the presence of the cold phase. (Hotspot and cold phase mass fractions have separate values and they are not mass-weighted.) As discussed

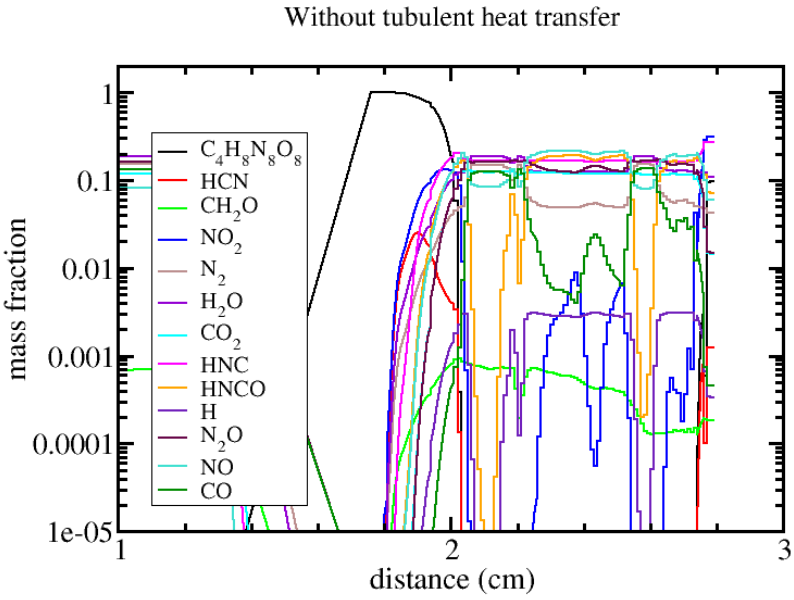

FIG. 4. Species mass fraction profiles at 3.88 μsec with thermal conduction only.

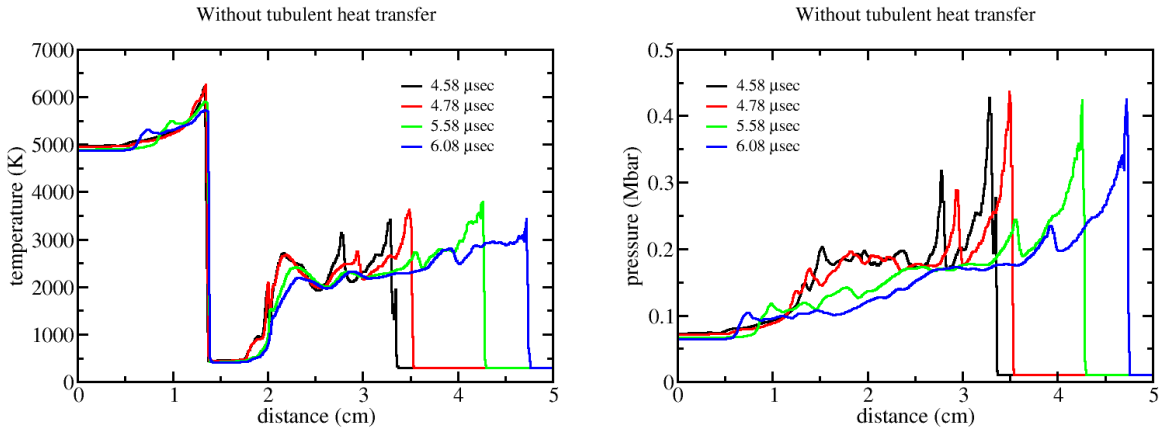

FIG. 5. Temperature and pressure profiles at 4.58, 4.78, 5.58, and 6.08 μsec with thermal conduction only.

in Ref. [13], detonation reactions are essentially complete in 5 computational zones.

We then carried out a simulation with turbulent heat transfer in both fractured HE and product gas. The critical Reynolds number Re_c has been taken to to be 500.0. Figure 8 shows temperature pressure profiles during the initial stage of the HE burning. Pressure rise starts propagating, and HE in the non-heated region does not show chemical reactions similar to the case without turbulence discussed above. At 3.08 μsec (brown), however, the temperature suddenly rises at around 2 cm, hinting that HE burn has started. This

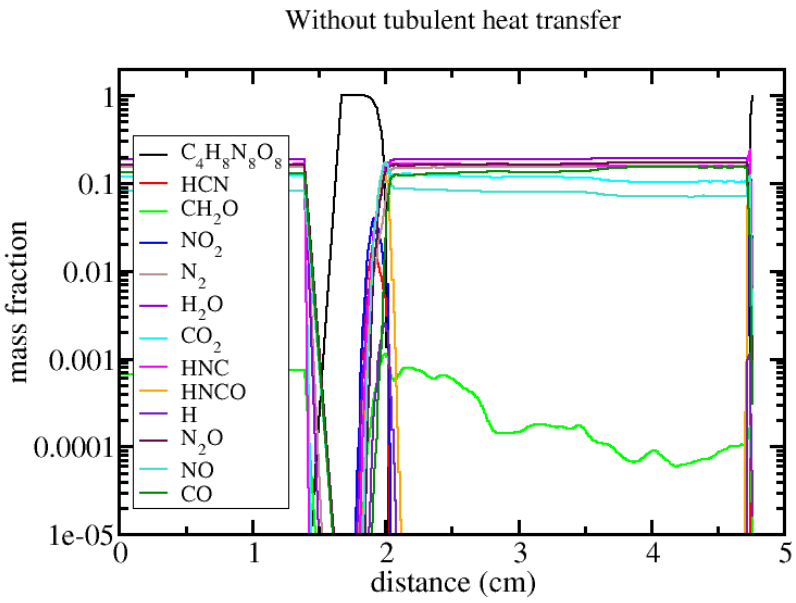

FIG. 6. Species mass fraction profiles at 6.08 μsec with thermal conduction only.

is confirmed by the active chemical reaction at 2.0 cm shown in Fig. 9. Note that no HE burning takes place at around 1.8 cm, suggesting that shockwave, not heat transfer from the heated region, is causing the onset of the chemical reactions at 2 cm.

Figure 9 reveals the contributions of both heating and hitting in the onset of HE burning. First, similar to Fig. 2, chemical reactions are caused by the temperature rise at around 1.3 cm due to the heat transfer from the heated region. However, both heat transfer from the heated region and the chemical energy release appear to be too slow to produce acceleration in HE burning. As a result, HE burning does not spread beyond the immediate neighborhood of the heated region. Note that the unburned HE region, into which HE burning spreads, is still in a solid state limiting heat transfer to conduction. That is, convection and turbulence have not been developed.

Compared to the temperature rise, shockwaves create more favorable conditions for chemical reactions such as increases in density and hotspots. In the present model [5], contribution of a hotspot is not expected to be large, since hotspot temperature is set to be relatively low. The role of hotspots will be studied when a more reliable hotspot model becomes available. In the present calculations, it thus appears that the substantial increases in chemical reactions are caused by the density increases due to the shock compression. As shown in Fig. 9, shockwave formation at some distance away from the heated region initiate the flame which accelerates and creates a detonation, as discussed below.

Formation of the flames with turbulent heat transfer are shown in Fig. 10. As the case without turbulent heat transfer discussed above, both temperature and pressure show rapid increases, signaling chemical energy release. However, peaks in both temperature and pressure appear to be larger (wider) than the non-turbulence case shown in Fig. 3. The case with turbulence nonetheless shows the same characteristics of the case without turbulence in the transition to detonation in spite of the enhanced heat transfer due to

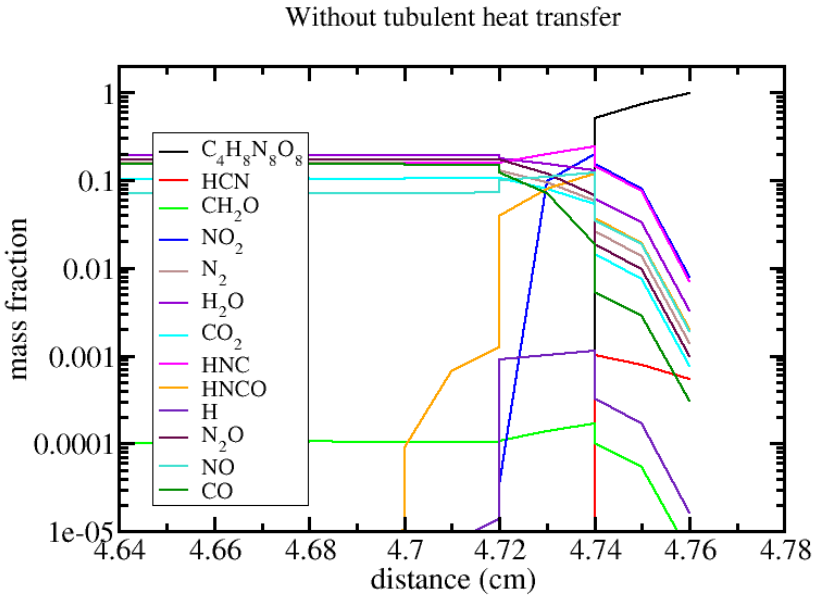

FIG. 7. Species mass fraction profiles around detonation wave at 6.08 μsec with thermal conduction only.

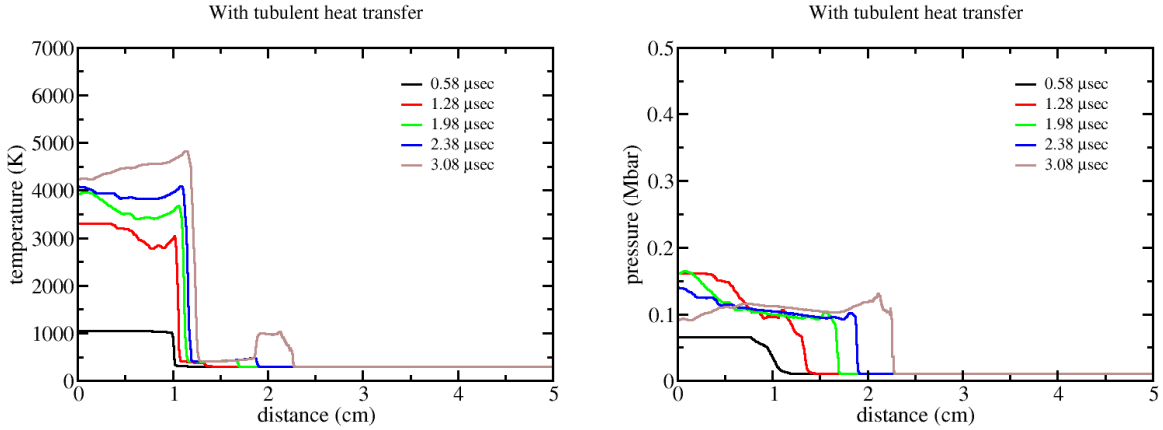

FIG. 8. Temperature and pressure profiles at 0.58, 1.28, 1.98, 2.38, and 3.08 μsec with turbulent heat transfer.

turbulence. (Increased heat transfer should increase the heating effect, relatively weakening the hitting effect.) As expected, it appears that the chemical reactions, or explosion of HE, in the heated region still is the stronger effect than the increased heat transfer, keeping the SDT-like process as the driving mechanism. (It is somewhat obvious since chemical energy release almost always dominates any cooling mechanism.) The leading (right) side of the second peak leads to the flame shock formation with characteristics discussed above.

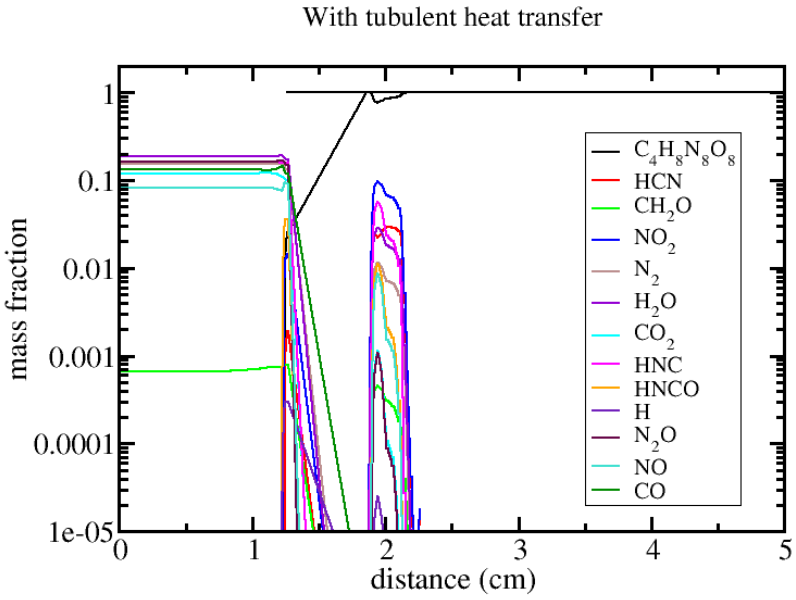

FIG. 9. Species mass fraction profiles at 3.08 μsec with turbulent heat transfer.

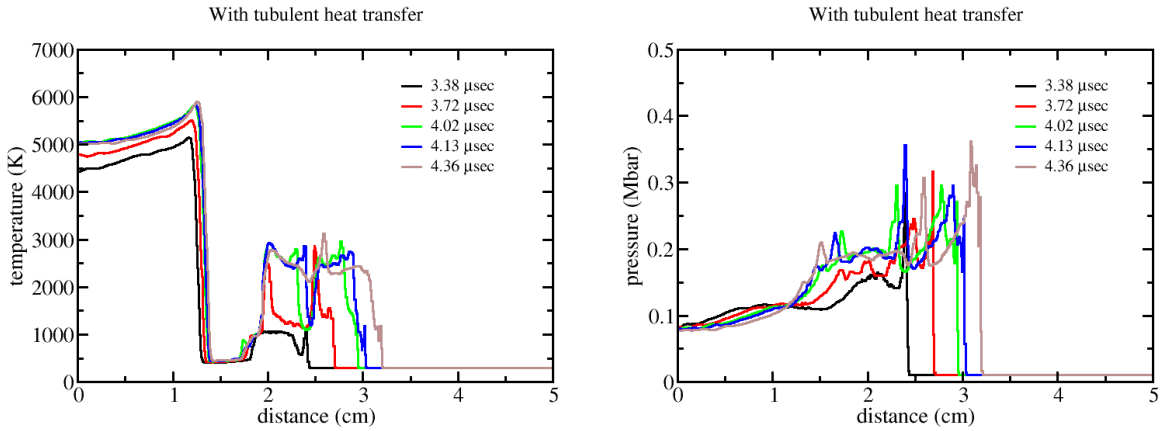

FIG. 10. Temperature and pressure profiles at 3.38, 3.72, 4.02, 4.13, and 4.36 μsec with turbulent heat transfer.

Species evolution shown in Fig. 11 also shows a similar behavior shown in Fig. 4.

Figure 12 shows development of a detonation wave by merging the leading and flame shockwaves for the case with turbulence, showing the identical behavior as the case of hitting [1]. The pressure profile at 4.82 μsec shows the "over-driven" behavior. This appears to be caused by the burning of unburned reactants. As the unburned reactants are consumed, the pressure profile quickly evolves into the "normal" detonation behavior. Species evolution shown in Fig. 13 also shows a similar behavior shown in Fig. 6.

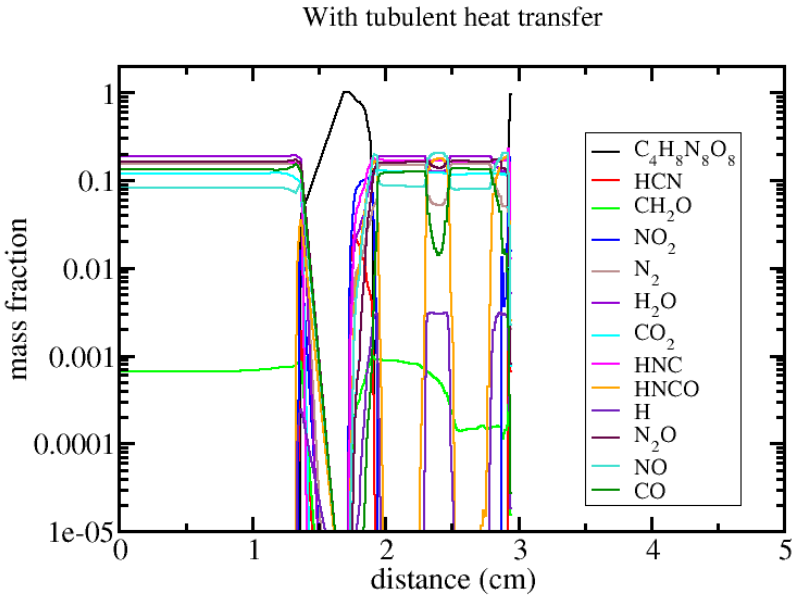

FIG. 11. Species mass fraction profiles at 4.02 μsec with turbulent heat transfer.

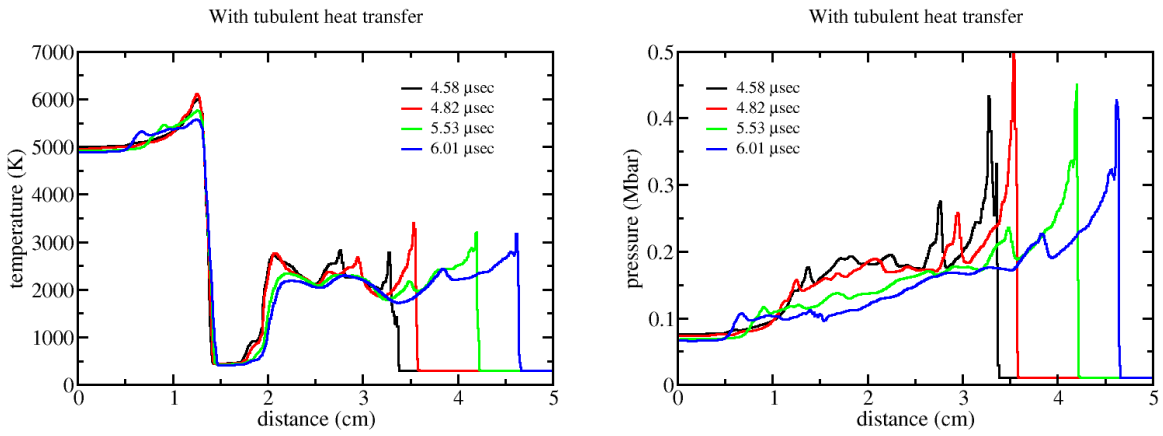

FIG. 12. Temperature and pressure profiles at 4.58, 4.82, 5.53, and 6.01 μsec with turbulent heat transfer.

IV. SUMMARY AND CONCLUDING REMARKS

As soon as HE burning starts, HE product gas rapidly fills the voids, pores, and cracks in fractured HE, and thermal convection becomes the dominating heat transfer mechanism. As HE burning progresses, turbulence would develop, enhancing the heat transfer. A turbulent heat transfer model has been developed for the fractured HE. In our model, turbulence developed in the fracture HE would become the initial turbulence for the HE

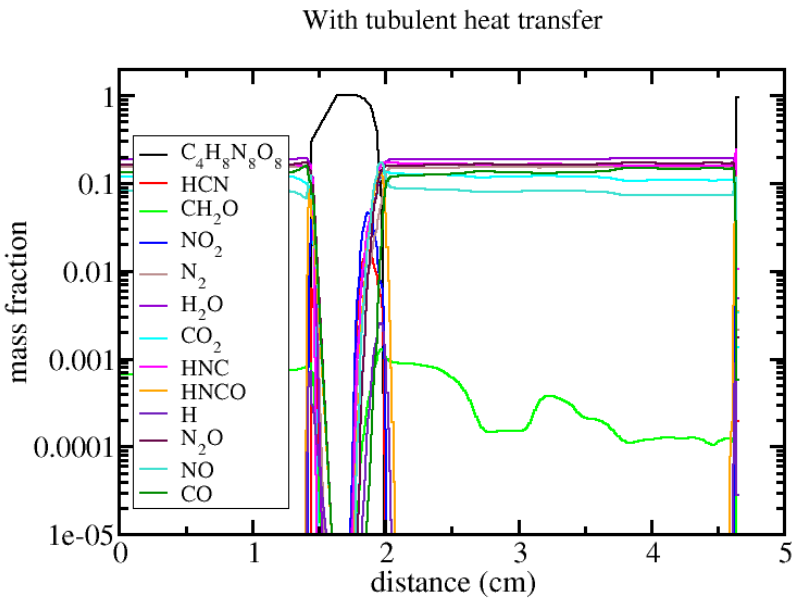

FIG. 13. Species mass fraction profiles at 6.01 μsec with turbulent heat transfer.

product gas, which then is modeled by a turbulence transport model composed of transport and dissipation of the turbulent kinetic energy. The present approach can be adopted by typical two-equation turbulence models. In the present report, this approach has been adapted to the KL model available in the BABBO code.

Numerical simulations of the onset of HE burning and transition to detonation have been performed with and without turbulent heat transfer. In these simulations, a region of HE is heated which caused a temperature rise in the neighboring HE. The expansion of the heated HE produced a pressure rise that propagated into the HE, forming a shockwave at some distance away from the heated region. Onset of HE burning has been observed in both regions: (1) the immediate neighbor region of the heated region where HE burning started due to the increased temperature, and (2) the region at some distance away from the heated HE where onset of burning occurs due to shock compression. This separation made it possible to isolate heating and hitting effects.

Simulations show that the flame acceleration (FA) and transition to detonation due to the shock compression similar to the FA and SDT by hitting previously discussed [1]. However, chemical reactions in the unburned region caused by the heat transfer rise appear to be relatively ineffective in the development of FA. Heat is transferred to the unburned HE with small porosity, which makes the convective and turbulent heat transfer ineffective. On the other hand, shock compression produces density increases, enhancing chemical reactions. The present computational results indicate that the shock compression leads to the development of the FA leading to detonation, and heating not accompanied by a pressure force (gradient) is ineffective. That is, processes similar to SDT appears to be a main driving mechanism even in the case of HE detonation due to heating.

Note that the heating rate is set relatively large in the present simulations in order to produce HE burning in a short amount of time. Slower heating will be studied with time-

implicit hydro scheme [14]. It is nonetheless expected that slower heating would still show similar characteristics to the present simulations, since the chemical energy release in the heated region would send out pressure pulses, forming a shockwave, and that the process like SDT would still be the important cause in the onset of HE burning and transition to detonation.

As mentioned throughout the present report, our hotspot model is in its infancy, and it tends to make the detonation more difficult at this point. As a result, it is expected that our approach would have difficulties in matching the run-to-detonation data. Improvements in the hotspot model is currently underway, and the effect of heating will be studied with an improved hotspot model in due course. Nonetheless, we again expect that the present characteristics would not change, likely with a quicker transition to detonation by the shock compression.

---

[1] C. H. Chang and A. J. Scannapieco, *Simulation of flame acceleration and deflagration-to-detonation transition with heat transfer in HE product and fractured HE*, report LA-UR-21-20155 (Los Alamos National Laboratory, 2021).

[2] B. F. Henson and L. Smilowitz, *Assessment of the application of the Henson-Smilowitz (HS) thermalkinetics model for energetic materials in current numerical tools*, Report unpublished (Los Alamos National Laboratory, 2016).

[3] C. Ticknor and J. A. Leiding, *MAGPIE: Reliable high explosive equation of state*, Tech. Rep. LA-UR-18-27689 (Los Alamos National Laboratory, 2018).

[4] B. Clements and X. Ma, *Mechanically Activated Thermal Chemistry (MATCH) Model for PAGOSA Users*, Report LA-CP-18-20483 (Los Alamos National Laboratory, 2018).

[5] C. H. Chang and A. J. Scannapieco, *Multiphase representation of hotspot formation and growth*, Report LA-UR-20-28334 (Los Alamos National Laboratory, 2020).

[6] B. E. Launder, A. Morse, W. Rodi, and D. B. Spalding, "Prediction of free shear flow – a comparison of the performance of six turbulence models," in *NASA SP-321*, Vol. 1 (National Aeronautics and Space Administration, Washington, D.C., 1973) p. 361.

[7] M. A. Leschziner and W. Rodi, "Computation of strongly swirling axisymmetric free jets," AIAA J. **22**, 1742 (1984).

[8] J. D. Ramshaw and C. H. Chang, "Computational fluid dynamics modeling of multicomponent thermal plasmas," Plasma Chem. Plasma Process. **12**, 299 (1992).

[9] G. Dimonte and R. Tipton, "K-L turbulence model for the self-similar growth of the Rayleigh-Taylor and Richtmeyer-Meshkov instabilities," Phys. Fluids **18**, 085101 (2006).

[10] B. D. Wood, X. He, and S. V. Apte, "Modeling turbulent flows in porous media," Ann. Rev. Fluid Mech. **52**, 171–203 (2020).

[11] S. Bastea, *Transport properties of fluid mixtures at high pressures and temperatures. Application to the detonation products of HMX*, Report UCRL-JC-13-145102 (Lawrence Livermore National Laboratory, 2002).

[12] J. Smargorinky, "General circulation experiments with the premitive equations. I. The basic experiment," Mon. Wea. Rev. **91**, 99 (1963).

[13] C. H. Chang and A. J. Scannapieco, *HMX detonation calculation using multi-reaction chain (Ver. 2)*, Report LA-UR-20-25658 (Los Alamos National Laboratory, 2020).

[14] A. J. Scannapieco and C. H. Chang, *Parallel implicit hydrodynamics for high explosive burn calculations*, report LA-UR-20-26036 (Los Alamos National Laboratory, 2020).